

Alma Mater Studiorum Università di Bologna
Archivio istituzionale della ricerca

Hierarchical chitinous matrices byssus-inspired with mechanical properties tunable by Fe(III) and oxidation

This is the final peer-reviewed author's accepted manuscript (postprint) of the following publication:

Published Version:

Montroni D., Palanca M., Morellato K., Fermani S., Cristofolini L., Falini G. (2021). Hierarchical chitinous matrices byssus-inspired with mechanical properties tunable by Fe(III) and oxidation. CARBOHYDRATE POLYMERS, 251, 116984-116993 [10.1016/j.carbpol.2020.116984].

Availability:

This version is available at: <https://hdl.handle.net/11585/802272> since: 2021-02-19

Published:

DOI: <http://doi.org/10.1016/j.carbpol.2020.116984>

Terms of use:

Some rights reserved. The terms and conditions for the reuse of this version of the manuscript are specified in the publishing policy. For all terms of use and more information see the publisher's website.

This item was downloaded from IRIS Università di Bologna (<https://cris.unibo.it/>).
When citing, please refer to the published version.

(Article begins on next page)

This is the final peer-reviewed accepted manuscript of:

Devis Montroni, Marco Palanca, Kavin Morellato, Simona Fermani, Luca Cristofolini, Giuseppe Falini “Hierarchical Chitinous Matrices Byssus-Inspired with Mechanical Properties Tunable by Fe(III) and Oxidation” Carbohydrate Polymers 251 (2021) 116984

The final published version is available online at:
<https://doi.org/10.1016/j.carbpol.2020.116984>

Terms of use:

Some rights reserved. The terms and conditions for the reuse of this version of the manuscript are specified in the publishing policy. For all terms of use and more information see the publisher's website.

This item was downloaded from IRIS Università di Bologna (<https://cris.unibo.it/>)

When citing, please refer to the published version.

Hierarchical Chitinous Matrices Byssus-Inspired with Mechanical Properties Tunable by Fe(III) and Oxidation

Devis Montroni^{*,1}, Marco Palanca², Kavin Morellato², Simona Fermani¹, Luca Cristofolini^{*,2} and Giuseppe Falini^{*,1}

¹ Department of Chemistry “Giacomo Ciamician”, Alma Mater Studiorum – University of Bologna, via F. Selmi 2, 40126 Bologna, Italy.

² Department of Industrial Engineering, Alma Mater Studiorum – University of Bologna, via Terracini 34, 40131 Bologna, Italy.

ABSTRACT: In this study the multi-scale hierarchical structure of the β -chitin matrix from the squid pen of *Loligo vulgaris* was used as substrate to prepare new bio-inspired materials. Finding inspiration from the byssus, aiming to mimic its peculiar mechanical properties, we chemically functionalized the β -chitin matrix with catechols, one of the main functional groups of the byssus. The obtained matrix preserved its multi-scale structural organization and was able to chelate reversibly Fe(III). Thus, it behaved as the byssus, acting as a metal cross-linkable matrix that upon metalation increased its Young's modulus, E (> 10 times). The functionalized matrix was also cross-linked by oxidation provoking an increase of the E (> 10 times) and first failure stress (> 5 times). The oxidation of the functionalized matrix followed by metalation slightly increased the material mechanical properties. In conclusion, we showed that specific bio-inspired functionalities can be added in a multi-scale and natural matrix tuning its mechanical properties without altering its overall organization.

Keywords: chitin; catechols; metal ions; hierarchical structures; bioinspired

*Corresponding authors. E-mail: giuseppe.falini@unibo.it (G. Falini)

devis.montroni2@unibo.it (D. Montroni)

luca.cristofolini@unibo.it (L. Cristofolini)

33 1. INTRODUCTION

34 Nature is able to produce materials with a multi-scale ordered hierarchical structure. Those materials can be
35 organic (mostly polymeric), inorganic, or organic-inorganic composites.(Eder, Amini, & Fratzl, 2018; Holland,
36 Blanford, Do, & Stein, 1999; Meyers et al., 2006; Seto et al., 2012) In them an ordered hierarchical structure
37 provides functional advantages compared to unstructured or disordered materials, such as mechanical
38 properties and biocompatibility.(Kennedy et al., 1999)

39 Chitin, poly-(β -(1–4)-N-acetyl-D-glucosamine), is the most abundant biopolymer in the animal kingdom. It is
40 also widely diffused among all the known species (being present in over 70 % of them), making it the most
41 common polymeric material used by nature.(Fernandez & Ingber, 2013; Montroni, Fermani, et al., 2019;
42 Montroni, Marzec, Valle, Nudelman, & Falini, 2019; Muzzarelli, 2013) It is present in a huge variety of
43 hierarchical organizations aimed to different purposes, being the most common for protective or structural
44 functions.(Al-Sawalmih et al., 2008; Ehrlich et al., 2010; Montroni, et al., 2019; Weaver et al., 2012; Yang et
45 al., 2019) Some examples of structured chitinous materials are found in sponges, where they occur as
46 nanostructured micro-porous skeletal elements.(Shaala et al., 2019; Wysokowski et al., 2015) In many
47 butterflies, such as the *Morpho* genus, chitin-based wings exhibit a photonic behaviour due to their periodic
48 structure.(Ghiradella & Radigan 1994; Kinoshita, Yoshika, Fujii, & Okamoto, 2002) In the squid pen of *Loligo*
49 *vulgaris* a hierarchical self-similar structure with micro-fibers of different size, composed themselves of
50 crystalline nano-fibrils, is observed and it is oriented along the long axis of the pen. Those fibers compose
51 different layers that overlap forming the squid pen.(Hunt & El Sherief, 1990)

52 Chitin has been widely applied in material science, drug delivery, medicine, optic, water remediation,
53 etc.(Anitha et al., 2014; Chabbi et al., 2020; Dev et al., 2010; Shams, Ifuku, Nogi, Oku, & Yano, 2011; K. Zhu
54 et al., 2019) This variety of fields of application is due to chitin's multi-properties, among which mechanical
55 resistance, biodegradability, biocompatibility, transparency, etc.(Pillai, Paul, & Sharma, 2009; Ravi Kumar,
56 2000; Singh, Dutta, Kumar, Kureel, & Rai, 2018; Tsai, Payne, & Shen, 2018) Chitin is frequently utilized in its
57 deacetylated form, named chitosan when the chitin's degree of acetylation (DA) is lower than 35 %.(Pillai et
58 al., 2009) Chitin is hardly soluble only in some strong polar organic solvents, while chitosan is easily
59 solubilized in acid solutions.(Ravi Kumar, 2000) Moreover, chitin has better mechanical properties than
60 chitosan, especially in the wet state, and a higher tendency to self-assemble in fibers.(Harmoudi et al., 2014;
61 Ifuku et al., 2013; Rathke & Hudson, 1994)

62 Nature's huge pool of efficient and performing materials has stimulated different bioinspired synthetic
63 approaches to emulate them. The synthesis of those new materials when performed by the bottom-up
64 approach fails in obtaining multiscale hierarchical ordered structures, as those produced by nature. An
65 alternative approach is using a natural material, in which the hierarchical structure is preserved at a defined
66 scale, and adding one or more levels of complexity. This approach allows combining the properties of the

67 two levels of complexity in a new functional material.(Ianiro et al., 2014) From the chemical point of view,
 68 the easiest way to add a property to a hierarchical material, as a polymeric one, is by functionalization with
 69 a chemical moiety. The wide application of chitinous materials has stimulated the development of different
 70 chemical routes to modify their properties.(Kurita, 2001; Sashiwa & Aiba, 2004) However, in these studies
 71 chitosan was mainly involved, even if reported as chitin.(Macquarrie & Hardy, 2005; Martin et al., 2002; Mi,
 72 Shyu, Chen, & Lai, 2002)

73 Among chemical functional groups, catechols have been widely used to obtain materials with high
 74 mechanical and adhesive properties, especially in wet environments.(J. Chen et al., 2020; Filippidi et al., 2017)
 75 This functionalization has been inspired by the studies on the byssus, the proteic thread produced by mussels
 76 to anchor to a substrate and resist to currents and waves. It presents catechol moieties, as 3,4-
 77 dihydroxyphenylalanine (DOPA), that are responsible for the thread's mechanical, self-healing, and adhesive
 78 properties.(Harrington, Masic, Holten-andersen, Waite, & Fratzl, 2010; Hwang et al., 2012; Montroni et al.,
 79 2018; Nicklisch & Waite, 2012)

80 Two catechol's chemical properties have stimulated its utilization in material sciences: i) the ability to chelate
 81 in reversible way transition metal ions as a bidentate ligand, and ii) the ability to cross-link covalently by the
 82 Michael addition reducing back to its dihydroxy state, upon oxidation to quinone.(Asghari et al., 2015; Guo,
 83 Ni, Wei, & Ren, 2015; L. Li, Smitthipong, & Zeng, 2015; Y. Li, Wen, Qin, Cao, & Wang, 2017; Qiao et al., 2014;
 84 H. Xu et al., 2012; Z. Xu, 2013) The catechol functionalization has been observed to increase the
 85 mucoadhesive property of materials.(Kim, Kim, Hyun, & Lee, 2015; L. Li et al., 2015; J. Xu, Strandman, Zhu,
 86 Barralet, & Cerruti, 2015) Chitosan functionalized with catechols produced a biocompatible mucoadhesive
 87 patch that was studied as drug delivery system.(Xu et al. 2015) Qiao at al. 2014, developed a solution of
 88 catechol-derived chitosan and Fe(III) that formed a gel upon an increment of pH.(Qiao et al., 2014) This
 89 material was studied as drug delivery system for Doxorubicin. Kim et al. 2015 tested the mucoadhesion
 90 capability of a chitin-catechol polymeric film defining it as "the most potent mucoadhesion polymers
 91 reported to date".(Kim et al., 2015) A catechol-chitosan coating was also applied to prevent oxidative stress
 92 to interfere with bone implant healing process.(W. Chen et al., 2017) Catechol-chitosan polymers were
 93 applied by Ryu et al. 2014 as a material self-converting in water insoluble dehydrated film, with application
 94 in food packaging.(Ryu, Jo, Koh, & Lee, 2014) Moreover, the metal-chelating ability of catechol-based
 95 matrices have also been exploited in water remediation.(Montroni et al., 2017) Most importantly, this
 96 chelating ability is also responsible for the self-healing properties of the byssus. In fact, along with traction
 97 the catechol-metal bond acts as sacrificial bond, avoiding initial critical damages, to reform after the stress is
 98 removed. Following this knowledge in 2017, Filippidi et al. developed a byssus inspired hydrogel exhibiting
 99 self-healing properties. (Filippidi et al., 2017)

100 The aim of our study is to modify chemically the hierarchically organized natural chitin matrix from the pen
101 of the squid *L. vulgaris*, increasing its complexity by functionalization with catechols. This material is actually
102 a good candidate for this synthetic approach. In fact, when an alkaline treatment at high temperatures is
103 used it can induce up to 45 % of deacetylation, producing glucosamine units, with minimal changes in
104 morphology and structure of the scaffold.(Montroni, Fermani, et al., 2019; Montroni, Sparla, Fermani, &
105 Falini, 2020) Those amino groups are supposed to be mainly located in amorphous regions or in the external
106 surface of the fibrils, and represent a perfect target for a coupling reaction. The final goal of this study is to
107 obtain a structured material at which the functional properties of catechols can be added, as occurs in the
108 byssus. The hypothesis is that the chemical functionalization will allow the control of the mechanical
109 properties upon reversible chelation of Fe(III), or by covalent cross-linking by oxidation.

110

111 2. EXPERIMENTAL SECTION

112 *2.1 Materials:* All reagents and solvents were purchased from Sigma Aldrich and utilized without any further
113 purification. Squid pens from *Loligo vulgaris* were collected from a local market. Once hydrated, the lateral
114 blades were isolated, cleaned with abundant distilled water (carefully eliminating eventual residual tissues)
115 and ethanol 70 vol.%, cleaned again using distilled water, and then stored dry in a desiccator.

116 *2.2 Synthesis of the matrices:* The squid pen was initially deproteinized inserting 2.5 g of squid pens,
117 previously washed as described, in 100 mL of a boiling 1 M NaOH solution and stirring gently for 1 h.(Ianiro
118 et al., 2014; Montroni et al., 2020) After that, the solution was changed with a fresh 1 M NaOH solution and
119 refluxed for 1 h. The obtained chitin films were washed at room temperature first with a 1 M NaOH solution
120 and then with distilled water until the washing solution had neutral pH. The films were stored dry in a
121 desiccator.

122 The chitin was successively deacetylated by adding 400 mg of the deproteinized chitin in 20 mL of a 5 M
123 NaOH boiling solution for 2 h under a gentle stirring.(Montroni, et al., 2019) The obtained chitin was then
124 washed at room temperature first with a 5 M NaOH solution and then with distilled water until washing
125 solution had neutral pH. The deacetylated chitin (DC) was stored dry in a desiccator.

126 The DC (800 mg) was then soaked in 90 mL of a pH 4.0 HCl solution for 15 minutes. In 45 mL of a 1:1 mixture
127 of ethanol and water, acidified to pH 4.0, 466 mg (2.5 eq. respect to the deacetylated glucosamine units) of
128 1-ethyl-3-(3-dimethylaminopropyl)carbodiimide and 266 mg (1.5 eq. respect to the deacetylated
129 glucosamine units) of 3,4-dihydroxyhydrocinnamic acid were solubilized and stirred for one minute.(Kim et
130 al., 2015; Qiao et al., 2014; Ryu et al., 2011; Zvarec, Purushotham, Masic, Ramanujan, & Miserez, 2013) The
131 ethanol/water solution was slowly dropped on the former one under stirring. The reaction mixture was set

132 on a rocking table in a dark room at 25 °C for 24 h. The catechol-functionalized deacetylated chitin matrices
133 (C_f-DC) were washed soaking them three times in an HCl pH 4.0 solution for 10 minutes. The matrices were
134 conserved wet in the pH 4.0 solution at 4 °C in the dark.

135 The crosslinking of the C_f-DC was induced soaking the previously prepared matrices in 200 mL of a carbonate
136 buffer 50 mM pH 9.5 for 24 h on a rocking table.(H. Lee, Dellatore, Miller, & Messersmith, 2007) The cross-
137 linked C_f-DC (CC_f-DC), were conserved in water at 4 °C in the dark.

138 The metal insertion in the matrices was performed using a 10 mM bicine buffer at pH 7 containing FeCl₃ or
139 VCl₃ in a 1:3 ratio between the deacetylated units and the metal ions.(Filippidi et al., 2017) The appropriate
140 amount of matrices were then soaked in the metal solution to get a 10 mg·mL⁻¹ dispersion of matrix in the
141 solution and set on a rocking table for 30 minutes. The specimens were then washed four times in water,
142 soaking the specimens for 5 minutes each time. The specimens were conserved in water at 4 °C in the dark.

143 The metal removal was performed soaking 10 mg·mL⁻¹ of sample in an EDTA 10 mM solution and setting the
144 solution on a rocking table for 30 minutes. The specimens were then washed four times in PremilliQ water,
145 soaking the specimens for 5 minutes each time, and conserved in PremilliQ water at 4 °C in the dark.

146 *2.3 Determination of the degree of acetylation:* The degree of acetylation (DA) of chitin was determined using
147 solid-state nuclear magnetic resonance (NMR). The NMR experiments were performed on a Bruker Advance
148 spectrometer operating at the frequency of 300 MHz for proton (equipped with a 4 mm MAS BB probe) using
149 the combined techniques of cross-polarization and magic angle spinning. Field strengths corresponding to
150 90° pulses of 4.5 μs were used for the matched spinlock cross-polarization transfer ¹H to ¹³C. The contact
151 time was 1 ms, and the recycle delay 10 s. A typical number of 500–3000 scans were acquired for each
152 spectrum. The chemical shifts were externally referred by setting the carbonyl resonance of glycine to 176.03
153 ppm. Glycine full width at half-height better than 27 Hz. The spinning speed was set at 8000 Hz for all
154 specimens. The assignment of NMR signals and the DA calculation was done according to literature.(Heux,
155 Brugnerotto, Desbrières, Versali, & Rinaudo, 2000)

156 *2.4 Swelling measurement:* The measure of the chitin specimen swelling in water was carried out first
157 weighting a dry specimen, conserved overnight in a desiccator under vacuum, and secondly weighting it after
158 soaking in water overnight, prior blotting it on a paper towel. The measures at pH 4 were performed using
159 an HCl solution at pH 4.0. Mass measurements were performed using a Sartorius CP225D (± 0.01 mg) on at
160 least 50 mg of initial dry specimen. The swelling measurements were performed at least on three
161 independent specimens.

162 *2.5 Spectroscopic analysis:* UV-Vis spectra were collected in transmission acquiring between 240 and 800 nm
163 with a 1 nm resolution, and an average time of 0.1 s using a Varian Cary 300 Bio spectrophotometer.

164 Raman spectra were acquired using a Renishaw Raman Invia spectrophotometer interfaced with a Leica
165 DMLM optical microscope. The spectrophotometer was equipped with a diode laser (780.0 nm, $P_{\max} = 300$
166 mW), an edge filter to remove the Rayleigh scattering, a monochromator (1200 lines·mm⁻¹), and a CCD
167 detector. The instrument was calibrated using a silicon wafer (520 cm⁻¹). The spectra were acquired summing
168 three spectra using a 1 % power and 10 s of acquisition.

169 *2.6 Synchrotron X-ray diffraction:* X-ray fiber diffraction diagrams were collected at XRD1 beamline, Elettra,
170 Trieste, Italy. Each frame was collected at the peak wavelength (0.9999 Å) using an exposure of 60 s. The X-
171 ray diffraction diagrams were analysed using Fit2D software.

172 *2.7 Scanning electron microscopy:* SEM images were acquired with a Philips SEM 515 using 15 eV. The wet
173 specimens were lyophilized, eventually cut with a scalpel to expose the section, glued on carbon tape, dried
174 overnight in a desiccator, and coated with 20 nm of gold prior to image them.

175 *2.8 Uniaxial tensile test:* Each specimen was cut in a proper dimension using scissors before the de-
176 proteination, maintained hydrated after the synthesis and tested hydrated. The actual width and thickness
177 of each hydrated specimen were measured after the synthesis using a SM-LUX POL microscope collecting
178 images with a 5.0 MP digital camera (Motic Moticam 5+). The images were analysed using ImageJ. Each
179 specimen was about 60 mm long, 5 mm wide, and 0.15-0.30 mm thick (the thickness varied between
180 specimens, because of the intrinsic variability of the initial biological specimens). Monotonic uniaxial tensile
181 tests were performed using a universal testing machine (Mod. 8032 with 8800 controller, Instron, UK) and
182 dedicated grips, leaving a free length of about 50 mm between the clamps. The tests were performed at
183 room temperature imposing a strain rate of 0.33 %·sec⁻¹ to all specimens (this resulted in an actuator speed
184 of the order of 10 mm·min⁻¹, depending on the actual gauge length of each specimen). As the curves were
185 rather linear until failure started, the following parameters could be calculated, taking into account the actual
186 dimensions of each specimen:

- 187 - The Young's modulus (E), defined as the slope of the linear part of the stress-strain curve;
- 188 - The stress ($\sigma_{1st\ failure}$) and strain ($\epsilon_{1st\ failure}$) when specimen failure started (yield, detected as a drop
189 of the force by 1 %);
- 190 - The maximum stress (σ_{\max});
- 191 - The work per unit volume required to reach yield ($Work_{1st\ failure}$) in J·mm⁻³.

192 All specimens failed in one of the two ways: either abrupt fracture, perpendicular to the specimen's axis, or
193 progressive unravelling of the fibers. The two modes of failure were not associated with specific specimen
194 groups. To this reason, the maximum elongation and the total work per unit volume were not evaluated
195 because they were not robust indicators of the specimens' behaviour. At least five specimens were tested

196 for each group. The Peirce criterion was adopted to detect and exclude outliers (15 % of the data had to be
197 excluded).(Ross, 2003) Normality was checked for each treatment group (sample) with the Kolmogorov-
198 Smirnov test. As the data did not follow a normal distribution, non- parametric statistical tests were applied
199 to each calculated mechanical parameters: Kruskal-Wallis test followed by a Dunn's post hoc.

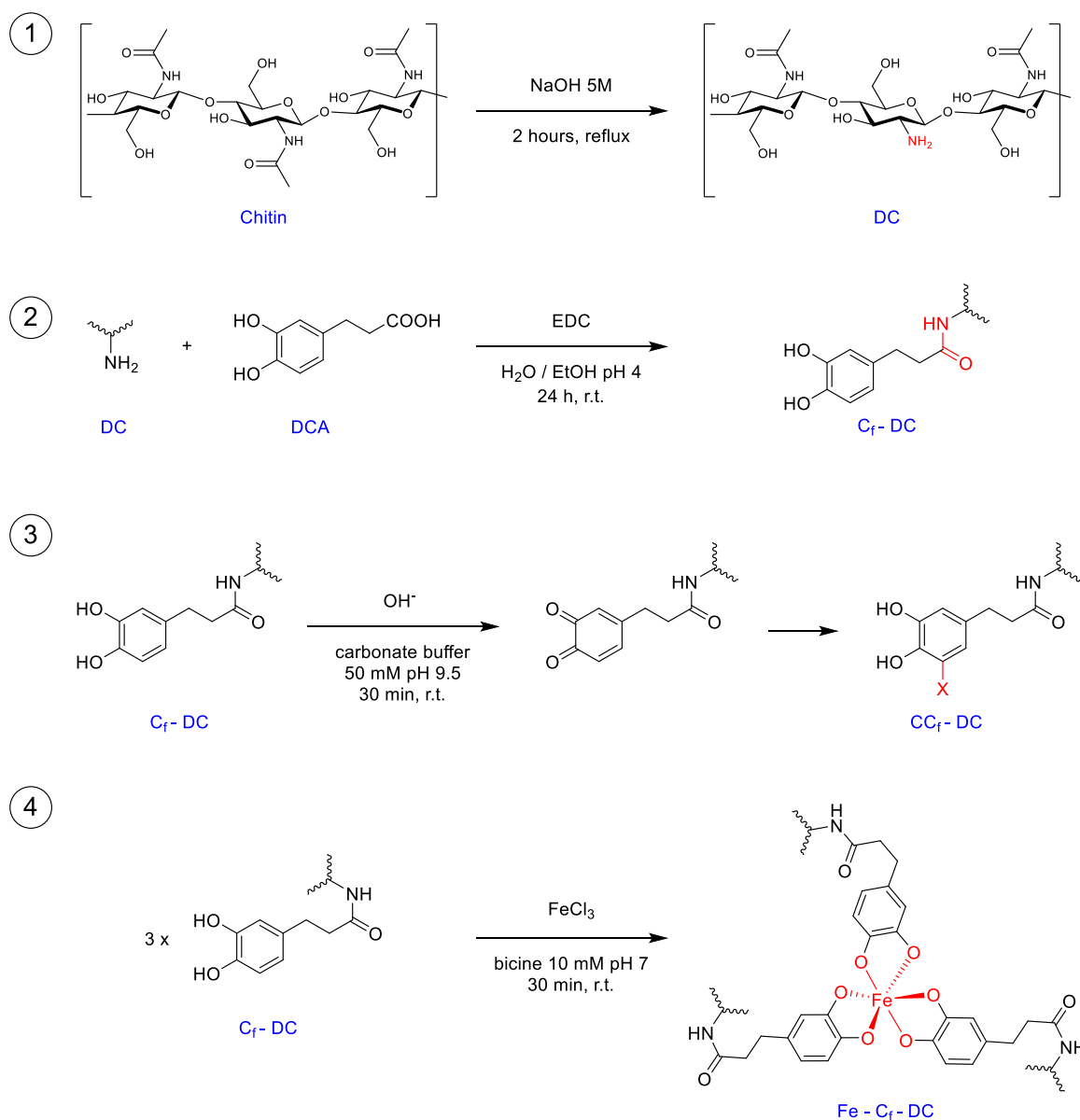
200

201 3. RESULTS

202 In this work the chitinous hierarchical structure of the squid pen of *L. vulgaris* was functionalized on the free
203 amino groups with catechols and then treated with Fe(III) and/or oxidized. A schematic of the different
204 matrices produced is reported in Figure S1.

205 The squid pen from *L. vulgaris* is a chitin based matrix composed of 40-50 wt.% of proteins.(Montroni et al.,
206 2019) The proteins were removed from the matrix using an aqueous 1 M NaOH solution treatment under
207 reflux for 2 h. This occurs without inducing any change in the morphology and structure of the chitinous
208 matrix in the pen. (Montroni, Fermani, et al., 2019; Montroni et al., 2020) After this first alkaline treatment,
209 the DA of chitin was about 88 %.(Montroni et al., 2019). A second alkaline treatment was performed using a
210 5 M NaOH solution under reflux for different times, see Figure 1 step 1, to increase the number of free amino
211 moieties in the matrix.(Montroni et al., 2019). The treatment was performed for 2 h, 8 h, or 24 h obtaining a
212 DA of 76.9 ± 0.6 %, 56 ± 1 %, and 32 ± 1 %, respectively (Figure S2). The 24 h treated chitosan matrix appeared
213 curly and not uniform, and was not used for further experiments. The two deacetylated chitin (DC) samples
214 had water swelling higher than 200 wt.%, Table S1, that was reached in less than 15 minutes. The second
215 step of the synthesis was the insertion of the catechol group, Figure 1 step 2. The reaction was performed by
216 applying a standard peptide coupling in water. The synthesis was optimized in pH and time as reported in the
217 SI (Figure S3). After this synthetic step, the catechol-functionalized DC (C_f -DC) obtained from the chitin
218 deacetylated for 8 h was in a gel state with swelling of 3000 ± 700 %, Table S1. Despite the birefringence of
219 the matrix appeared conserved, it was impossible to perform uniaxial tensile tests on this set of specimens
220 due to difficulties in handling, even after Fe(III) treatment or crosslinking. Thus, the successive experiments
221 were performed only using the C_f -DC obtained from the chitin deacetylated for 2 h.

222



223

224 **Figure 1.** Scheme of the synthetic steps to functionalize the matrix. 1) Chitin partial de-acetylation, to obtain
 225 the DC. 2) DC functionalization with catechols, to obtain the C_F-DC. 3) C_F-DC basic crosslinking, to obtain
 226 the CC_F-DC, where X can represents a heteroatom (such as oxygen from –OH groups, or nitrogen from –NH₂
 227 groups) or another aromatic ring. 4) Metal insertion in the C_F-DC, to obtain Fe-C_F-DC.

228

229 The Fe(III) chelation in the C_F-DC was optimized testing different pHs of bicine buffer, as reported in Figure
 230 S4. UV-Vis spectra of the C_F-DC before and after Fe(III) insertion showed a typical broad catechol–iron peak
 231 appearing between 500 and 700 nm in the metal treated matrices.(Guo et al., 2015) This peak came along
 232 with a shift of the catechol signal from 280 to 288 nm. Only a weak signal of the o-quinone (oxidized catechol)
 233 at 400 nm was observed.(Guo et al., 2015) After Fe(III) insertion, the matrix appeared of a bright blue (Figure
 234 2).

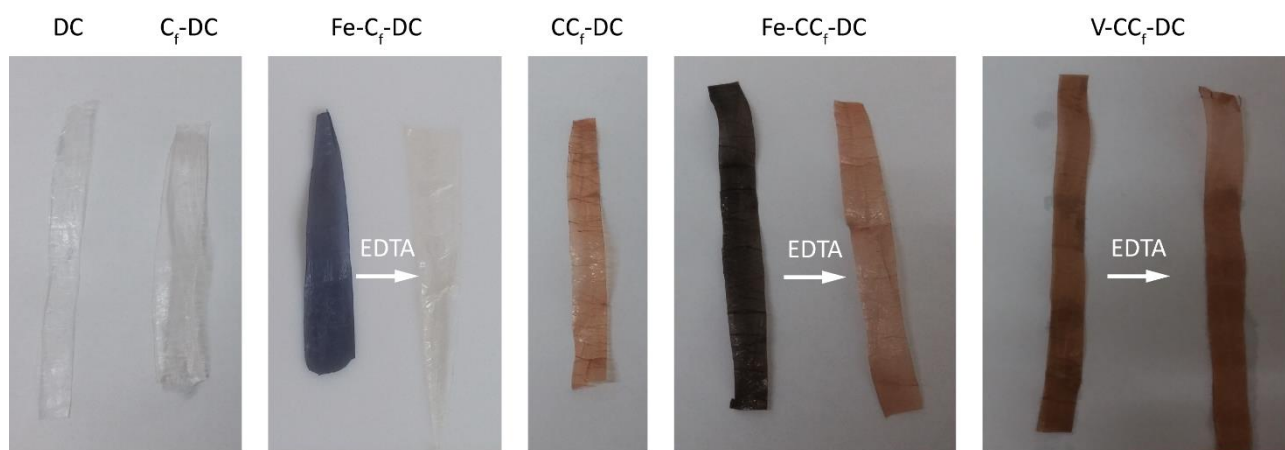


Figure 2. Picture of the different matrices obtained in the different stages of the synthesis. Scale bar 5 mm.

The coloration disappeared after treatment with EDTA and the UV-Vis spectrum restored as in the C_f -DC. The presence of catechol-iron(III) complexes was also confirmed using Raman spectroscopy, Figure 3. (Guo et al., 2015) No significant change in the swelling was observed after metal insertion, Table S1.

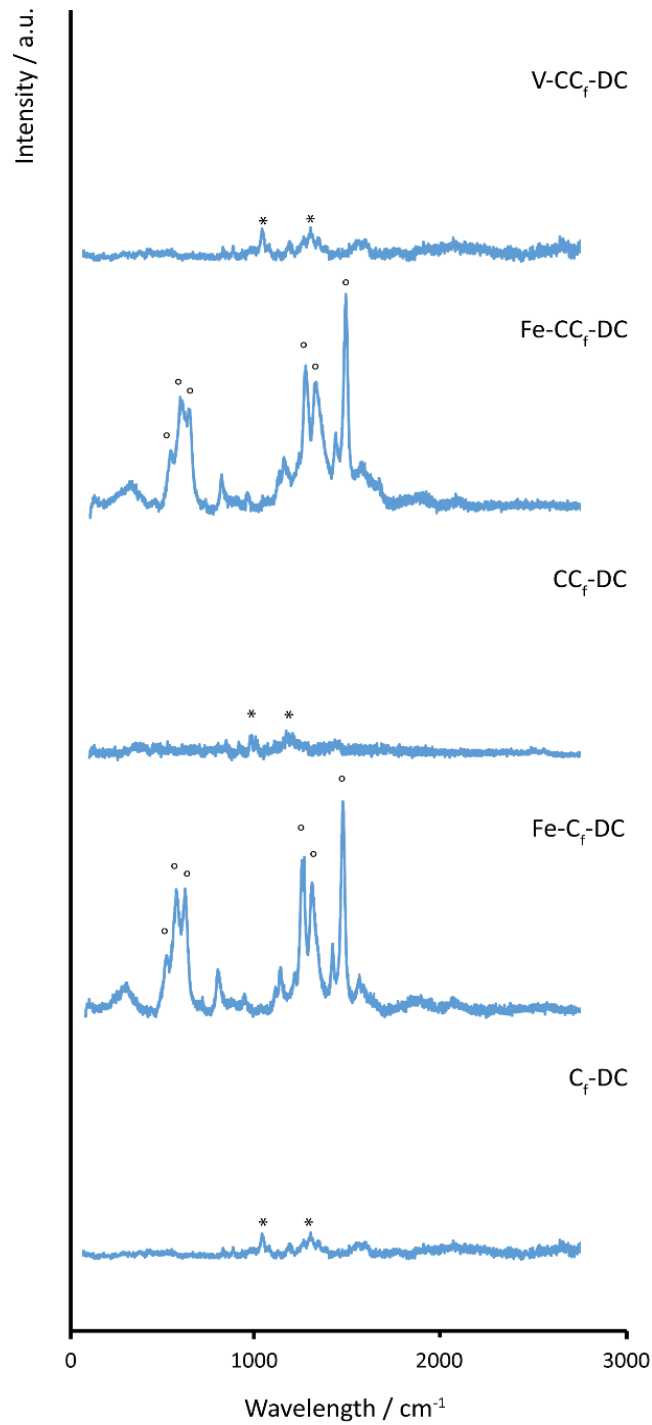


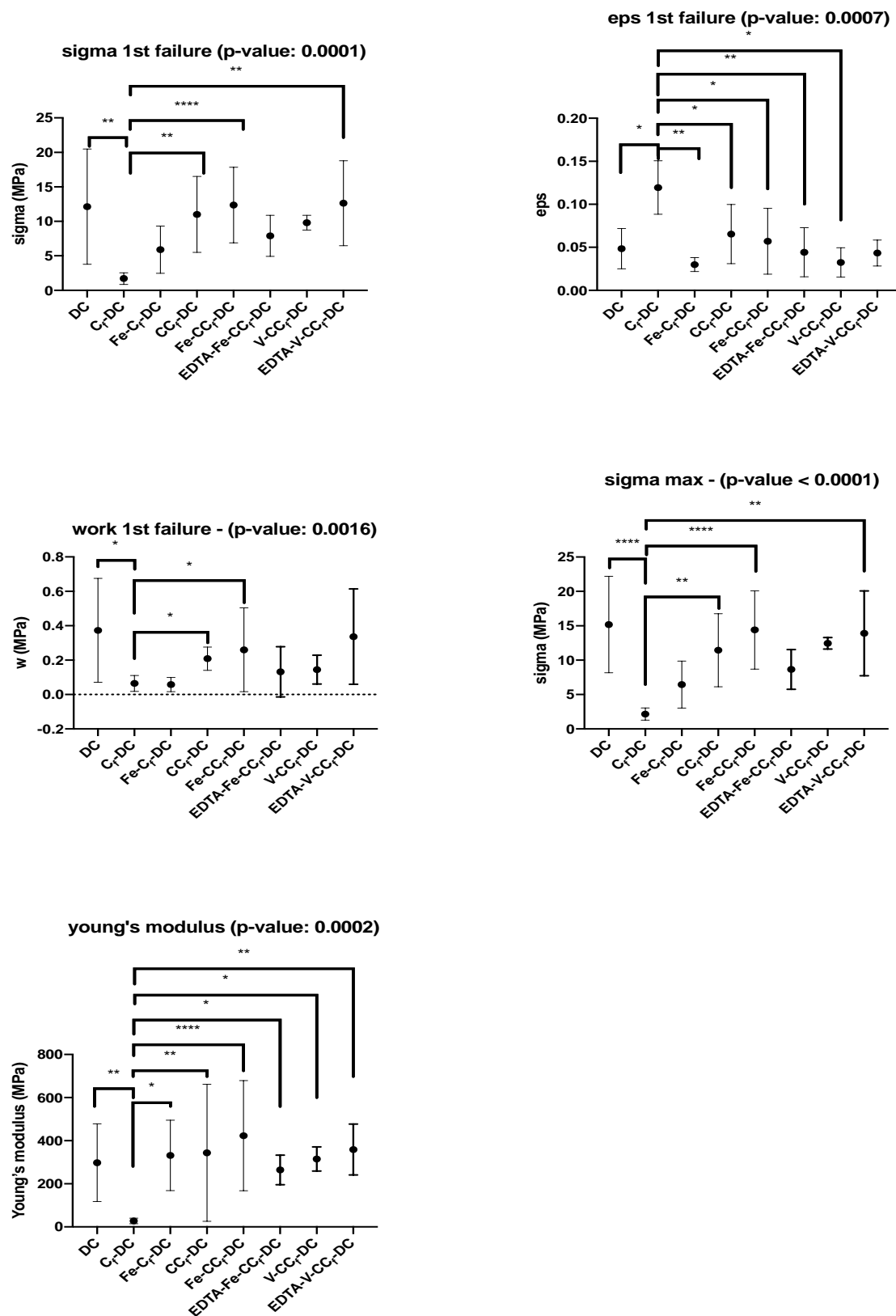
Figure 3. Raman spectra of the different matrices. According to literature, all the samples containing iron show only catechol-Fe signals (°), as the Fe-O bond vibrations in the 500–700 cm⁻¹.(Guo et al., 2015) Chitin signals (*) were observed in all the samples.(Kaya et al., 2017)

The mechanical properties were evaluated for each sample group (Table 1, Figure 4). In particular, the C_f-DC showed, in comparison with the DC, lower first failure ($\sigma_{1st\ failure}$), maximum stress (σ_{max}), work and Young's

249 modulus (E), and higher first failure elongation ($\epsilon_{1st\ failure}$). The Fe-C_f-DC showed, with respect to C_f-DC, an
250 increase of the $\sigma_{1st\ failure}$ and of the σ_{max} (not statistically significant), and at the same time a significant
251 decrease of $\epsilon_{1st\ failure}$, with a consequent higher E (> 10 times), both comparable with the DC.

252 Catechols can also undergo covalent crosslinking by oxidation, Figure 1, step 3. The C_f-DC was covalently
253 cross-linked using a basic environment as an alternative way to tune its mechanical properties. A basic
254 environment was chosen instead of stronger oxidative conditions to get a slow oxidation that would allow
255 the matrix to physically reorganize its structure along the reaction. Moreover, this slower process would help,
256 avoiding as much as possible, to re-oxidize the catechols after the cross-linking. Three different pHs were
257 tested, pH 7, 9.5 and 14, for two different times, 24 h and 48 h. The best mechanical parameter results were
258 obtained using the pH 9.5 for 24 h, which showed a higher σ_{max} and E, and a lower swelling ($300 \pm 100\%$),
259 diagnostic for a proper cross-linking, compared to the other conditions (see SI for more details). The values
260 were comparable with those of DC. If compared to the C_f-DC an increment of more than 10 times in E, 3 times
261 in the work, and over 5 times in the $\sigma_{1st\ failure}$ and σ_{max} were observed.

262



263

264 **Figure 4.** Mechanical data of the different matrices synthetized. For each mechanical data the overall
 265 significance of the Kruskal-Wallis test is reported. The level of Dunn's post-hoc statistical significance is
 266 reported between groups. ****: p-value < 0.0001; ***: p value < 0.001; **: p-value < 0.01; * = p-value <
 267 0.05.

269 **Table 1.** Mechanical parameters of the matrices synthesized.

Sample	$\sigma_{1st\ Failure}$ (MPa)	$\epsilon_{1st\ Failure}$	Work _{1st Failure} (MPa)	σ_{max} (MPa)	E (MPa)
DC	12 ± 8	0.07 ± 0.02	0.4 ± 0.3	15 ± 7	300 ± 100
C _f -DC	1.7 ± 0.8	0.12 ± 0.03	0.06 ± 0.04	2.2 ± 0.8	30 ± 10
Fe-C _f -DC	6 ± 3	0.03 ± 0.01	0.06 ± 0.04	7 ± 3	300 ± 200
CC _f -DC	11 ± 5	0.07 ± 0.03	0.21 ± 0.06	12 ± 5	300 ± 300
Fe-CC _f -DC	12 ± 5	0.06 ± 0.04	0.2 ± 0.2	14 ± 6	400 ± 200
EDTA-Fe-CC _f -DC	8 ± 3	0.05 ± 0.03	0.1 ± 0.2	9 ± 3	260 ± 60
V-CC _f -DC	10 ± 1	0.03 ± 0.02	0.15 ± 0.08	12.4 ± 0.8	320 ± 60
EDTA-V-CC _f -DC	13 ± 5	0.05 ± 0.02	0.4 ± 0.3	14 ± 4	360 ± 90

270

271 Successively, Fe(III) was inserted in the cross-linked matrices in a 3:1 molar ratio between the free amine
 272 groups and Fe(III) (Fe-CC_f-DC), Figure 1 step 4. The UV-Vis absorption peak for catechol-Fe(III) complexes was
 273 observed and the Raman spectra showed signals of catechol-Fe(III) complexes (Figure 3 and S6). The Fe-CC_f-
 274 DC was then treated using EDTA inducing a loss of the UV-Vis absorption band of the catechol-Fe complex
 275 and a change in the color, Figure 2.

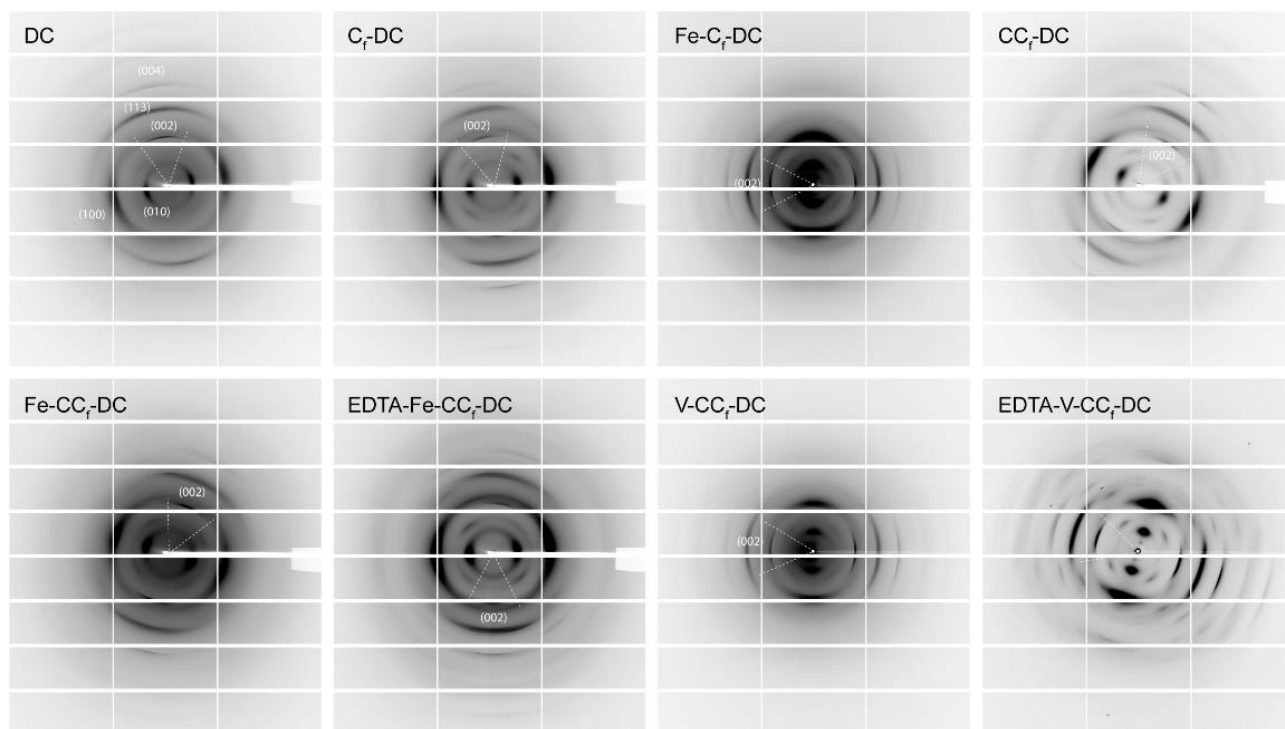
276 The Fe-CC_f-DC showed a slight improvement (about 20 %) of the E, $\sigma_{1st\ failure}$, σ_{max} , and Work, and an equal
 277 decrease in the $\epsilon_{1st\ failure}$ compared to the CC_f-DC, but all the differences between the two groups were not
 278 statistically significant. A decrease in the swelling to 260 ± 40 % was observed. Once treated with EDTA, the
 279 parameters became more similar to the ones of CC_f-DC.

280 To test the effect of massive oxidation on the system in comparison to the metal coordination we exposed
 281 the CC_f-DC to V(III) that has a chelating ability similar to Fe(III), but that instead of complexation induces
 282 oxidation on the catechols. The matrix exposed to V(III) (V-CC_f-DC) showed a broad peak at about 550 nm
 283 (Figure S6) but no signals of the catechol-V(III) complex were detected using Raman spectroscopy (Figure 3).

284 The V-CC_f-DC showed similar mechanical properties to the CC_f-DC, despite a drop of the swelling to 230 ± 10
 285 % occurred due to the further cross-linking of the matrix. Contrary to the Fe(III) treated sample, the V-CC_f-DC
 286 one when treated with EDTA did not change properties (Figure 4; Tables S1 and S2).

287 The overall structural integrity of the matrices was investigated by fiber XRD using synchrotron radiation,
 288 Figure 5 and Table S2. The diffraction images showed how all specimens maintained a comparable fibril
 289 alignment, evaluated by the azimuthal angular spread of the reflection (002), Table S2. Indeed, the full width
 290 at half maximum along the angle ranged between 30° and 34°, without any evident trend. The diffracted
 291 intensity changed among the samples, Table S2. This could be due to a diverse crystallinity among them,
 292 which reflected the variability always present in biological samples. Those containing Fe(III) or vanadium ions
 293 showed a higher diffracted intensity, probably due to the positive contribute of the metal ions to the
 294 coherent scattering of the structure. A slight structural reorganization was observed in the inter-planar
 295 distance associated to the reflection (010). When the strongest catechol oxidation was performed (V-CCf-DC
 296 sample) this distance was maximum at 11.1 Å, while in the starting sample (DC) was 10.7 Å.

297



298

299 **Figure 5.** Synchrotron X-ray fiber diffraction images of the samples. In DC the Miller index of the reflection
 300 are indicated. The diffraction peaks were indexed according to the monoclinic unit cell of β -chitin (Gardner,
 301 & Blackwell, 1975). The dotted lines limit the angular spread of the reflection (002).

302

303 Interestingly, the presence of Fe(III) (Fe-C_f-DC) on the catechol functionalized chitin (C_f-DC) induced an
 304 increase of the inter-planar distance from 10.5 Å to 10.9 Å.

305 The morphology and micro-structural organization of the specimens were examined using SEM, observing
 306 the specimen's longitudinal section and external surface (Figure 6). The initial DC scaffold presented an
 307 almost homogenous surface with a parallel fibrous organization and a lamellar structure in the section. As

308 reported in Montroni et al. 2019 and 2020, the alkaline treatment does not interfere with the chitinous
309 structure of the squid pen, therefore the DC is representative of the initial multi-scale structure of the pristine
310 pen.(Montroni, Fermani, et al., 2019; Montroni et al., 2020) A SEM image of a pristine squid pen is reported
311 in Figure S9. The specimen surface was almost unaltered in all specimens examined becoming a little more
312 homogenous compared to the DC but still showing an aligned fibrous arrangement. A difference in
313 morphology was observed in sample C_f-DC where it was not possible to observe the lamellar structure in the
314 section, which appeared in a foam-like state. This structure was restored after the metal insertion, in sample
315 Fe-C_f-DC, or alkaline cross-linking, in sample CC_f-DC. A clustering of the layers was observed after Fe(III) and
316 V(III) treatment of the CC_f-DC. This clustering disappeared after EDTA treatment in sample Fe-CC_f-DC (EDTA-
317 Fe-CC_f-DC) but not in sample V-CC_f-DC (EDTA-V-CC_f-DC).

318 As observed in Figure 2 the overall macro-structure of the squid pen was conserved along all the synthetic
319 steps.

320

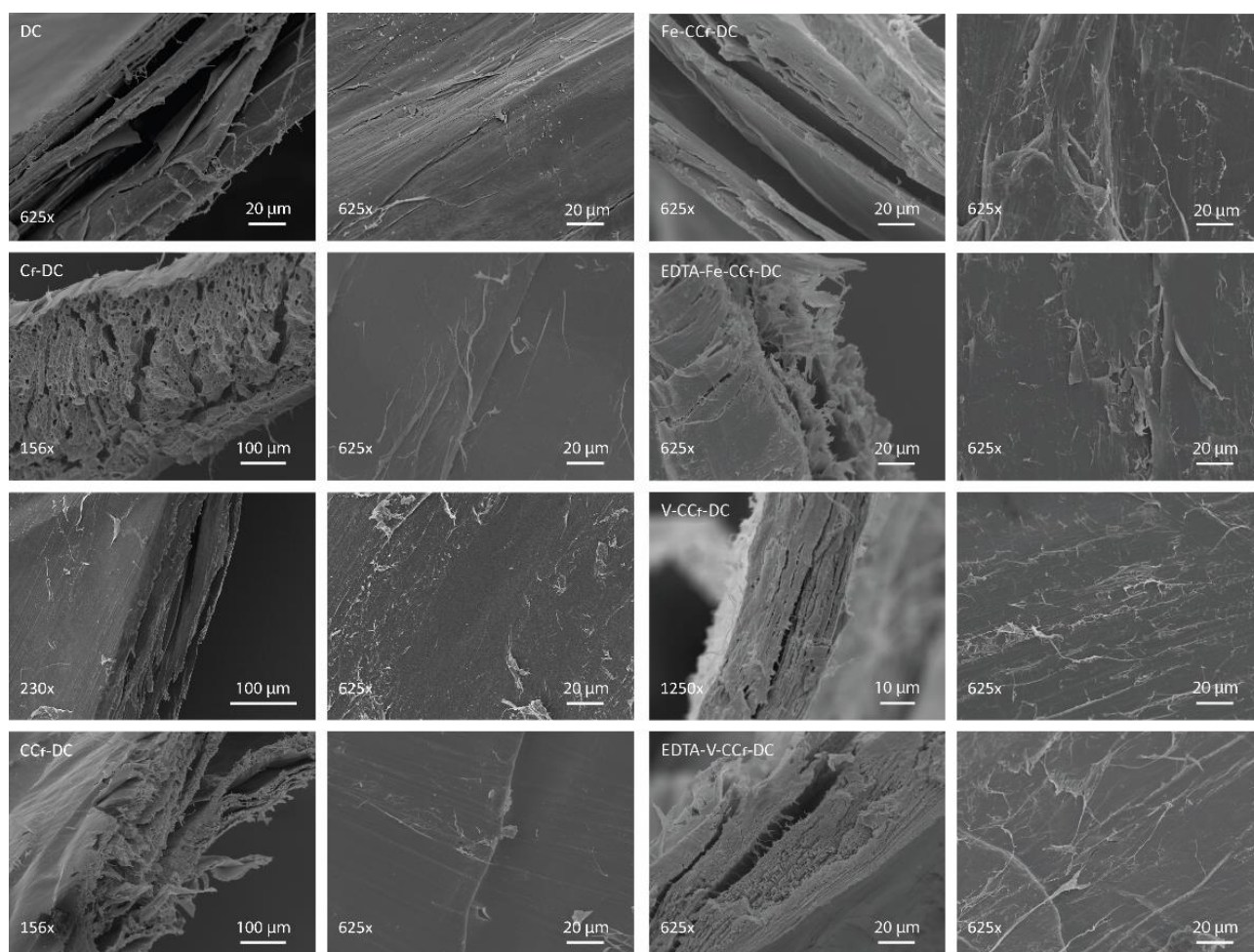


Figure 6. SEM images of the matrices synthetizes. For each specimen is reported, on the left, an image of a longitudinal section showing the lamellar structure of the chitinous matrix and, on the right, an image of the sample surface.

4. DISCUSSION

The emulation of the complex hierarchical structures produced by the organism is the main goal of biomimetic and bioinspired syntheses. The achievement of this goal has involved the research activity of a plethora of scientists. Although many biomimetic materials have been produced, the faithful reproduction of the evolutionary evolved hierarchical structure of natural materials has been rarely, if ever, achieved. Approaching this research, we realized this difficulty and decided to change the synthetic approach. We used as matrix a hierarchical natural material, not obtainable in laboratory and with the complexity of the variability typical of the natural materials. In it, we added a level of complexity by chemical functionalization. Accordingly, this work produced a family of chitin-based materials from the squid pen, in which the structure of the chitin matrix is preserved and catechol functionalities bioinspired from mussel's byssus thread have been added.

337 The catechol functionalization has been reported for chitosan gels, although in several cases was named
338 chitin functionalization despite the fact that chitin does not form gels in water.(Guo et al., 2015; Kim et al.,
339 2015; Kim, Ryu, Lee, & Lee, 2013; Qiao et al., 2014; Ryu et al., 2011; J. Xu et al., 2015; Zvarec et al., 2013) No
340 work has been reported on actual chitin (with a high DA), or on a chitin hierarchically organized material.
341 Filippidi et al. used also a synthetic approach inspired by mussel byssus, incorporating sacrificial, reversible
342 catechol-Fe(III) cross-links into loosely cross-linked epoxy network.(Filippidi et al., 2017) In this case, a
343 hierarchical structure was missing in the epoxy network.

344 The functionalization with catechols has required an optimization that was governed by the conflicting needs
345 of preserving the native structure of the matrix and maximize its functionalization with catechols. This goal
346 has been achieved as shown by the diffractometric and microscopic investigations and by the observation
347 that the covalently catechol functionalized matrix was able to bind reversibly Fe(III). As consequence of the
348 functionalization, a decrease of the evaluated mechanical properties was observed without a radical change
349 of the crystalline structure of the matrix. This decrease in the mechanical parameters was predictable
350 considering that the specimens were tested hydrated and the functionalized matrix contained over two times
351 the water of the DC. After metal insertion the structurally and crystalline intact matrix obtained, Fe-C_r-DC,
352 differed significantly from the C_r-DC in E (> 10 times) appearing as a stiffer material, but not able to absorb
353 more energy.

354 The catechols offer also the possibility to generate crosslinking by oxidation with the formation of covalent
355 bonds.(Guo et al., 2015; Pillar, Zhou, & Guzman, 2015) In nature, catechol cross-linked protein networks,
356 such as sclerotized cuticle and byssal threads of the mussel, have been shown to exhibit excellent mechanical
357 properties.(A. Miserez, Schneberk, Sun, W. F., & H. J., 2008; Z. Xu, 2013) According to this information, C_r-DC
358 was covalently cross-linked to tune the mechanical resistance in the matrix and induce a slight clustering of
359 the material to favour metal bridges formation. The material obtained showed a marked stiffer behaviour
360 compared to the functionalized matrix having comparable mechanical parameters to that of DC. It is also
361 remarkable that cross-linking reduced variability inside the sample for most mechanical parameters, except
362 for the Young's modulus. The decrease in swelling observed was a validation that a cross-linking occurred.
363 This matrix showed only a slight reversible increase in the stress and work, upon chelation of Fe(III). Thus,
364 the Fe(III) chelation did not add cross-linking useful for the increase of the mechanical performances.

365 The effect of a high level of cross-linking in the matrix was studied in comparison to Fe(III) cross-linking. V(III)
366 was used as oxidant since it has coordination chemistry similar to Fe(III) and the presence of catechol-V(III)
367 complexes can be efficiently detected by Raman spectroscopy.(Montroni et al., 2018) The spectrum excluded
368 the presence of this complex. In addition the UV-Vis spectrum indicated the presence of V(III).(C. Choi et al.,
369 2017; N. H. Choi, Kwon, & Kim, 2013) The V(III) treated matrix did not show significant differences with the
370 CC_r-DC except in the swelling, as a hint that the matrix undergoes a further cross-linking. These results show

371 how the exposure to a stronger oxidant did not further increase the mechanical performances of the matrix
372 despite a higher cross-linking occurred. This might be due to the formation of bridges not influencing the
373 mechanical properties.

374 As mentioned, the overall structure was maintained in all the matrices obtained. The XRD pattern was
375 examined for all the matrices and the crystalline structure appeared mostly unaltered. Only a small change
376 on the periodicity associate to the inter-planar distance among chitin planes, the (010) planes, was observed
377 in the Fe(III) cross-linked and oxidized samples. This agreed with the hindrance of these chemical moieties.
378 The microscopic images showed that fibril alignment of the structures was maintained in all the synthetic
379 steps. In agreement with the previous observations after Fe(III) insertion, a reversible clustering of the
380 lamellas was observed, supporting the proved metal-induced cross-linking. The un-expected morphological
381 change observed in the C_r-DC, was probably induced by the lyophilisation following highly swelled state, in
382 fact it was not detected in secondary matrices.

383 The experiments performed in this research showed that the improvement of mechanical properties of a
384 hierarchical structured matrix, like the β -chitin squid pen one, can be achieved using two different strategies,
385 i.e. by formation of coordination bonds with metal ions and by covalent cross-linking. The discussed data
386 show that oxidative treatment with V(III) on alkaline cross-linked matrices does not affect significantly the
387 mechanical properties. This latter observation indicated that the alkaline treatment already saturated the
388 cross-links useful for the improvement of the mechanical properties, as Young modulus of about 10 times.
389 Similarly, in a recent study surface-deacetylated chitin nanofibers that were cross-linked by reaction between
390 quinone and amino groups increased almost 10-fold higher tensile strength.(C. Chen, Li, Yano, & Abe, 2019)

391 The mechanical performances did not change significantly in the alkaline cross-linked matrices after metal
392 ion treatment, although a positive trend was observed. Since the formation of coordination bonds occurs on
393 the same functional groups, only a low improvement is expected. These two cross-link strategies have been
394 widely used by organisms that do not use minerals in their structural tissue. Indeed, while the metal ion
395 coordination bonds is observed for example in the byssus,(Harrington et al., 2010) the catechol cross-linking
396 has been reported in their powerful chitin based mouthparts of the *Dosidicus gigas* (jumbo squids).(Ali
397 Miserez, Li, Waite, & Zok, 2007) Although these studies find inspiration from sclerotization or tanning of
398 chitin in hard tissues of many organisms, they can give hits on the chemical conditions that organisms use to
399 achieve optimal mechanical properties and be of inspiration for synthetic processes. (Cohen, 2010; K. Lee,
400 Prajatelista, Hwang, & Lee, 2015; A. Miserez et al., 2008; K. Y. Zhu, Merzendorfer, Zhang, Zhang, &
401 Muthukrishnan, 2016)

402

403 5. CONCLUSIONS

404 We successfully synthesized different advanced materials using a synthetic approach in which a hierarchical
405 natural matrix (i.e. the deproteinized squid pen of *L. vulgaris*) has been functionalized finding inspiration from
406 nature (i.e. byssus).

407 The functionalized matrices were all able to coordinate Fe(III). The material's mechanical properties were
408 tuneable and/or reversible based on the kind of cross-linking, metal ion chelation (reversible) or oxidative
409 (irreversible), induced on the catechol functional groups. The obtained material, according to the exposed
410 environment, changed from stiffer to softer materials (with E ranging from 30 to 400 MPa and σ_{\max} from 2.2
411 to 14 MPa), therefore acting as a stimuli responsive material. Moreover, the two different cross-linking gave
412 materials with different mechanical behaviour. Iron insertion showed mostly an influence on the E (increasing
413 it from 30 to 300 MPa), while oxidation affected all the mechanical parameters (shifting $\epsilon_{1st\ Failure}$ from 0.12
414 to 0.07 %, σ_{\max} from 2.2 to 12 MPa, and E from 30 to 300 MPa). These chemical processes, when differently
415 performed, can allow a diverse customization of the material.

416 These chelating tuneable matrices might find application and not only in: medicine, as grafts or wound
417 healing materials (being catechols a mucoadhesive enhancing group); water remediation, as chelating
418 matrices; sensors, as metal-responsive materials.

419 In conclusion, this work shows for the first time that hierarchically organized matrices can be functionalized
420 without altering its multi-scale organization, to get functional materials. This approach could lead to new
421 advanced functional materials combining nature's precisely controlled structure and human's chemistry
422 expertise.

423

424 ASSOCIATED CONTENT

425 **Supporting Information**

426 Synthetic details; spectroscopic characterization of the materials; results of the microstructural analysis;
427 data on mechanical and physical characterization of the materials.

428

429 ACKNOWLEDGEMENTS

430 This research did not receive any specific grant from funding agencies in the public, commercial, or not-for-
431 profit sectors. We thank the XRD1 beamline, Elettra, Trieste, Italy for the collection of the X-ray diffraction
432 images. GF, SF and DM thank the Consorzio Interuniversitario di Ricerca in Chimica dei Metalli nei Sistemi
433 Biologici for the support.

434

435 REFERENCES

- 436 Al-Sawalmih, A., Li, C., Siegel, S., Fabritius, H., Yi, S., Raabe, D., ... Paris, O. (2008). Microtexture and
 437 chitin/calcite orientation relationship in the mineralized exoskeleton of the american lobster.
 438 *Advanced Functional Materials*, 18, 3307–3314. <https://doi.org/10.1002/adfm.200800520>
- 439 Anitha, A., Sowmya, S., Kumar, P. T. S., Deepthi, S., Chennazhi, K. P., Ehrlich, H., ... Jayakumar, R. (2014).
 440 Chitin and chitosan in selected biomedical applications. *Progress in Polymer Science*, 39, 1644–1667.
 441 <https://doi.org/10.1016/j.progpolymsci.2014.02.008>
- 442 Asghari, A., Ameri, M., Baraee, B., Rajabi, M., Bakherad, M., & Amoozadeh, A. (2015). Mechanistic
 443 investigation of the electro- oxidation of catechols in the presence of N -methylbenzylamine at room
 444 temperature : synthesis of new quinone derivatives. *Progress in Reaction Kinetics and Mechanism*,
 445 40(1), 77–85. <https://doi.org/10.3184/146867815X14199390979580>
- 446 Chabbi, J., Aqil, A., Katir, N., Vertruyen, B., Jérôme, C., Lahcini, M., & El Kadib, A. (2020). Aldehyde-
 447 conjugated chitosan-graphene oxide glucodynamers: Ternary cooperative assembly and controlled
 448 chemical release. *Carbohydrate Polymers*, 230(June 2019).
 449 <https://doi.org/10.1016/j.carbpol.2019.115634>
- 450 Chen, C., Li, D., Yano, H., & Abe, K. (2019). Bioinspired hydrogels : Quinone crosslinking reaction for chitin
 451 nano fi bers with enhanced mechanical strength via surface deacetylation. *Carbohydrate Polymers*,
 452 207(November 2018), 411–417. <https://doi.org/10.1016/j.carbpol.2018.12.007>
- 453 Chen, J., Peng, Q., Peng, X., Han, L., Wang, X., Wang, J., & Zeng, H. (2020). Recent Advances in Mechano-
 454 Responsive Hydrogels for Biomedical Applications. *ACS Applied Polymer Materials*, 2(3), 1092–1107.
 455 <https://doi.org/10.1021/acsapm.0c00019>
- 456 Chen, W., Shen, X., Hu, Y., Xu, K., Ran, Q., Yu, Y., ... Cai, K. (2017). Surface functionalization of titanium
 457 implants with chitosan-catechol conjugate for suppression of ROS-induced cells damage and
 458 improvement of osteogenesis. *Biomaterials*, 114, 82–96.
 459 <https://doi.org/10.1016/j.biomaterials.2016.10.055>
- 460 Choi, C., Kim, S., Kim, R., Choi, Y., Kim, S., Jung, H. young, ... Kim, H. T. (2017). A review of vanadium
 461 electrolytes for vanadium redox flow batteries. *Renewable and Sustainable Energy Reviews*, 69, 263–
 462 274. <https://doi.org/10.1016/j.rser.2016.11.188>
- 463 Choi, N. H., Kwon, S. K., & Kim, H. (2013). Analysis of the oxidation of the V(II) by dissolved oxygen using UV-
 464 visible spectrophotometry in a vanadium redox flow battery. *Journal of the Electrochemical Society*,
 465 160(6), A973–A979. <https://doi.org/10.1149/2.145306jes>
- 466 Cohen, E. (2010). Chitin Biochemistry: Synthesis, Hydrolysis and Inhibition. In *Advances in Insect Physiology*

(1st ed., Vol. 38). [https://doi.org/10.1016/S0065-2806\(10\)38005-2](https://doi.org/10.1016/S0065-2806(10)38005-2)

Dev, A., Mohan, J. C., Sreeja, V., Tamura, H., Patzke, G. R., Hussain, F., ... Jayakumar, R. (2010). Novel carboxymethyl chitin nanoparticles for cancer drug delivery applications. *Carbohydrate Polymers*, 79, 1073–1079. <https://doi.org/10.1016/j.carbpol.2009.10.038>

Eder, M., Amini, S., & Fratzl, P. (2018). Biological composites—complex structures for functional diversity. *Science*, 362(6414), 543–547. <https://doi.org/10.1126/science.aat8297>

Ehrlich, H., Simon, P., Carrillo-cabrera, W., Bazhenov, V. V., Botting, J. P., Ilan, M., ... Paasch, S. (2010). *Insights into Chemistry of Biological Materials : Newly Discovered Silica-Aragonite-Chitin Biocomposites in Demosponges*. (9), 1462–1471. <https://doi.org/10.1021/cm9026607>

Fernandez, J. G., & Ingber, D. E. (2013). Bioinspired chitinous material solutions for environmental sustainability and medicine. *Advanced Functional Materials*, 23, 4454–4466. <https://doi.org/10.1002/adfm.201300053>

Filippidi, E., Cristiani, T. R., Eisenbach, C. D., Waite, J. H., Israelachvili, J. N., Ahn, B. K., & Valentine, M. T. (2017). Toughening elastomers using mussel- inspired iron-catechol complexes. *Science*, 358, 502–505.

Ghiradella, H., & Radigan, W. (n.d.). Development of Butterfly Scales. *J. Morph.*, 150, 279–298.

Ghiradella, Helen. (1994). Structure of butterfly scales: Patterning in an insect cuticle. *Microscopy Research and Technique*, 27, 429–438. <https://doi.org/10.1002/jemt.1070270509>

Guo, Z., Ni, K., Wei, D., & Ren, Y. (2015). Fe³⁺-induced oxidation and coordination cross-linking in catechol–chitosan hydrogels under acidic pH conditions. *RSC Adv.*, 5(47), 37377–37384. <https://doi.org/10.1039/C5RA03851K>

Harmoudi, H. El, Gaini, L. El, Daoudi, E., Rhazi, M., Boughaleb, Y., Mhammedi, M. A. El, ... Bakasse, M. (2014). Removal of 2,4-D from aqueous solutions by adsorption processes using two biopolymers : chitin and chitosan and their optical properties. *Optical Materials*, 36, 1471–1477.

Harrington, M. J., Masic, A., Holten-andersen, N., Waite, J. H., & Fratzl, P. (2010). Iron-Clad Fibers : A Metal-Based Biological Strategy for Hard Flexible Coatings. *Science*, 328, 216–221.

Heux, L., Brugnerotto, J., Desbrières, J., Versali, M. F., & Rinaudo, M. (2000). Solid State NMR for Determination of Degree of Acetylation of Chitin and Chitosan. *Biomacromolecules*, 1, 746–751. <https://doi.org/10.1021/bm000070y>

Holland, B. T., Blanford, C. F., Do, T., & Stein, A. (1999). Synthesis of highly ordered, three-dimensional, macroporous structures of amorphous or crystalline inorganic oxides, phosphates, and hybrid

498 composites. *Chemistry of Materials*, 11(3), 795–805. <https://doi.org/10.1021/cm980666g>

499 Hunt, S., & El Sherief, A. (1990). A periodic structure in the “pen” chitin of the squid *Loligo vulgaris*. *Tissue*
500 *and Cell*, 22(2), 191–197. [https://doi.org/10.1016/0040-8166\(90\)90021-Z](https://doi.org/10.1016/0040-8166(90)90021-Z)

501 Hwang, D. S., Harrington, M. J., Lu, Q., Masic, A., Zeng, H., & Waite, J. H. (2012). Mussel foot protein-1
502 (mcfp-1) interaction with titania surfaces(). *Journal of Materials Chemistry*, 22(31), 15530–15533.
503 <https://doi.org/10.1039/C2JM32439C>

504 Ianiro, A., Giosia, M., Fermani, S., Samorì, C., Barbalinardo, M., Valle, F., ... Falini, G. (2014). Customizing
505 Properties of β -Chitin in Squid Pen (Gladius) by Chemical Treatments. *Marine Drugs*, 12, 5979–5992.
506 <https://doi.org/10.3390/md12125979>

507 Ifuku, S., Ikuta, A., Egusa, M., Kaminaka, H., Izawa, H., Morimoto, M., & Saimoto, H. (2013). Preparation of
508 high-strength transparent chitosan film reinforced with surface-deacetylated chitin nanofibers.
509 *Carbohydrate Polymers*, 98, 1198–1202. <https://doi.org/10.1016/j.carbpol.2013.07.033>

510 Kaya, M., Mujtaba, M., Ehrlich, H., Salaberria, A. M., Baran, T., Amemiya, C. T., ... Labidi, J. (2017). On
511 chemistry of γ -chitin. *Carbohydrate Polymers*, 176, 177–186.
512 <https://doi.org/10.1016/j.carbpol.2017.08.076>

513 Kennedy, W. R., Dubey, N., Navarro, X., Wendelschafer-Crabb, G., Ceballos, D., & Tranquillo, R. T. (1999).
514 Magnetically Aligned Collagen Gel Filling a Collagen Nerve Guide Improves Peripheral Nerve
515 Regeneration. *Experimental Neurology*, 158, 290–300. <https://doi.org/10.1006/exnr.1999.7111>

516 Kim, K., Kim, K., Hyun, J., & Lee, H. (2015). Chitosan-catechol : A polymer with long-lasting mucoadhesive
517 properties. *Biomaterials*, 52, 161–170.

518 Kim, K., Ryu, J. H., Lee, D. Y., & Lee, H. (2013). Bio-inspired catechol conjugation converts water-insoluble
519 chitosan into a highly water-soluble, adhesive chitosan derivative for hydrogels and LbL assembly.
520 *Biomaterials Science*, 1, 783–790. <https://doi.org/10.1039/c3bm00004d>

521 Kinoshita, S., Yoshika, S., Fujii, Y., & Okamoto, N. (2002). Photophysics of Structural Color in the Morpho
522 Butterflies Shuichi. *Forma*, 17(1), 103–121.

523 Kurita, K. (2001). Controlled functionalization of the polysaccharide chitin. *Prog. Polym. Sci.*, 26, 1921–1971.

524 Lee, H., Dellatore, S. M., Miller, W. M., & Messersmith, P. B. (2007). Mussel-Inspired Surface Chemistry for
525 Multifunctional Coatings. *Science*, 318, 426–430. <https://doi.org/10.1017/CBO9781107415324.004>

526 Lee, K., Prajatelista, E., Hwang, D. S., & Lee, H. (2015). Role of Dopamine Chemistry in the Formation of
527 Mechanically Strong Mandibles of Grasshoppers. *Chemistry of Materials*, 27(19), 6478–6481.
528 <https://doi.org/10.1021/acs.chemmater.5b01680>

529 Li, L., Smitthipong, W., & Zeng, H. (2015). Mussel-inspired hydrogels for biomedical and environmental
530 applications. *Polymer Chemistry*, 6, 353–358. <https://doi.org/10.1039/C4PY01415D>

531 Li, Y., Wen, J., Qin, M., Cao, Y., & Wang, W. (2017). Single-Molecule Mechanics of Catechol-Iron
532 Coordination Bonds. *ACS Biomater. Sci. Eng.*, 3(6), 979–989.
533 <https://doi.org/10.1021/acsbiomaterials.7b00186>

534 Macquarrie, D. J., & Hardy, J. J. E. (2005). Applications of functionalized chitosan in catalysis. *Industrial and*
535 *Engineering Chemistry Research*, 44, 8499–8520. <https://doi.org/10.1021/ie050007v>

536 Martin, L., Wilson, C. G., Koosha, F., Tetley, L., Gray, A. I., Senel, S., & Uchegbu, I. F. (2002). The release of
537 model macromolecules may be controlled by the hydrophobicity of palmitoyl glycol chitosan
538 hydrogels. *Journal of Controlled Release*, 80, 87–100. [https://doi.org/10.1016/S0168-3659\(02\)00005-6](https://doi.org/10.1016/S0168-3659(02)00005-6)

539 Meyers, M. A., Lin, A. Y. M., Seki, Y., Chen, P., Kad, B. K., & Bodde, S. (2006). Structural Biological
540 Composites : An Overview. *JOM*, 58, 35–41.

541 Mi, F. L., Shyu, S. S., Chen, C. T., & Lai, J. Y. (2002). Adsorption of indomethacin onto chemically modified
542 chitosan beads. *Polymer*, 43, 757–765. [https://doi.org/10.1016/S0032-3861\(01\)00580-8](https://doi.org/10.1016/S0032-3861(01)00580-8)

543 Miserez, A., Schneberk, T., Sun, C., W. F., Z., & H. J., W. (2008). The Transition from Stiff to Compliant
544 Materials in Squid Beaks. *Science*, 319, 1816–1819.

545 Miserez, Ali, Li, Y., Waite, J. H., & Zok, F. (2007). Jumbo squid beaks: Inspiration for design of robust organic
546 composites. *Acta Biomaterialia*, 3(1), 139–149. <https://doi.org/10.1016/j.actbio.2006.09.004>

547 Montroni, D., Fermani, S., Morellato, K., Torri, G., Naggi, A., Cristofolini, L., & Falini, G. (2019). β -Chitin
548 samples with similar microfibril arrangement change mechanical properties varying the degree of
549 acetylation. *Carbohydrate Polymers*, 207, 26–33. <https://doi.org/10.1016/j.carbpol.2018.11.069>

550 Montroni, D., Marzec, B., Valle, F., Nudelman, F., & Falini, G. (2019). β -Chitin Nanofibril Self-Assembly in
551 Aqueous Environments. *Biomacromolecules*, 20(6), 2421–2429.
552 <https://doi.org/10.1021/acs.biomac.9b00481>

553 Montroni, D., Piccinetti, C., Fermani, S., Calvaresi, M., Harrington, M. J., & Falini, G. (2017). Exploitation of
554 mussel byssus mariculture waste as a water remediation material. *RSC Advances*, 7, 36605–36611.
555 <https://doi.org/10.1039/c7ra06664c>

556 Montroni, D., Sparla, F., Fermani, S., & Falini, G. (2020). Influence of proteins on mechanical properties of a
557 natural chitin-protein composite. *Acta Biomaterialia*. <https://doi.org/10.1016/j.actbio.2020.04.039>

558 Montroni, D., Valle, F., Rapino, S., Fermani, S., Calvaresi, M., Harrington, M. J., & Falini, G. (2018).
559 Functional Biocompatible Matrices from Mussel Byssus Waste. *ACS Biomaterials Science and*

560 *Engineering*, 4, 57–65. <https://doi.org/10.1021/acsbiomaterials.7b00743>

561 Montroni, D., Zhang, X., Leonard, J., Kaya, M., Amemiya, C., Falini, G., & Rolandi, M. (2019). Structural
562 characterization of the buccal mass of *Ariolimax californicus* (Gastropoda; Stylommatophora). *PLoS*
563 *ONE*, 14(8), e0212249.

564 Muzzarelli, R. A. (2013). *Chitin*. Elsevier.

565 Nicklisch, S. C. T., & Waite, J. H. (2012). Mini-review: The role of redox in Dopa-mediated marine adhesion.
566 *Biofouling*, 28(8), 865–877. <https://doi.org/10.1080/08927014.2012.719023>

567 Pillai, C. K. S., Paul, W., & Sharma, C. P. (2009). Chitin and chitosan polymers: Chemistry, solubility and fiber
568 formation. *Progress in Polymer Science*, 34(7), 641–678.
569 <https://doi.org/10.1016/j.progpolymsci.2009.04.001>

570 Pillar, E. A., Zhou, R., & Guzman, M. I. (2015). Heterogeneous Oxidation of Catechol. *J. Phys. Chem.*, 119,
571 10349–10359. <https://doi.org/10.1021/acs.jpca.5b07914>

572 Qiao, H., Sun, M., Su, Z., Xie, Y., Chen, M., Zong, L., ... Ping, Q. (2014). Kidney-specific drug delivery system
573 for renal fibrosis based on coordination-driven assembly of catechol-derived chitosan. *Biomaterials*,
574 35, 7157–7171. <https://doi.org/10.1016/j.biomaterials.2014.04.106>

575 Rathke, T. D., & Hudson, S. M. (1994). Review of Chitin and Chitosan as Fiber and Film Formers. *Journal of*
576 *Macromolecular Science , Part C*, 34(3), 374–437.

577 Ravi Kumar, M. N. . (2000). A review of chitin and chitosan applications. *Reactive and Functional Polymers*,
578 46(1), 1–27. [https://doi.org/10.1016/S1381-5148\(00\)00038-9](https://doi.org/10.1016/S1381-5148(00)00038-9)

579 Ross, S. M. (2003). Peirce’s criterion for the elimination of suspect experimental data. *Journal of*
580 *Engineering Technology*, 20(2), 38–41.

581 Ryu, J. H., Jo, S., Koh, M. Y., & Lee, H. (2014). Bio-inspired, water-soluble to insoluble self-conversion for
582 flexible, biocompatible, transparent, catecholamine polysaccharide thin films. *Advanced Functional*
583 *Materials*, 24, 7709–7716. <https://doi.org/10.1002/adfm.201402250>

584 Ryu, J. H., Lee, Y., Kong, W. H., Kim, T. G., Park, T. G., & Lee, H. (2011). *Catechol-Functionalized Chitosan /*
585 *Pluronic Hydrogels for Tissue Adhesives and Hemostatic Materials †*. 2653–2659.

586 Sashiwa, H., & Aiba, S. I. (2004). Chemically modified chitin and chitosan as biomaterials. *Progress in*
587 *Polymer Science*, 29, 887–908. <https://doi.org/10.1016/j.progpolymsci.2004.04.001>

588 Seto, J., Ma, Y., Davis, S. A., Meldrum, F., Gourrier, A., Kim, Y. Y., ... Cölfen, H. (2012). Structure-property
589 relationships of a biological mesocrystal in the adult sea urchin spine. *Proceedings of the National*

590 *Academy of Sciences of the United States of America*, 109(10), 3699–3704.
 591 <https://doi.org/10.1073/pnas.1109243109>

592 Shaala, L. A., Asfour, H. Z., Youssef, D. T. A., 'Zółtowska-Aksamitowska, S., Wysokowski, M., Tsurkan, M., ...
 593 Ehrlich, H. (2019). New Source of 3D Chitin Scaffolds : The Red Sea Demosponge Pseudoceratina
 594 arabica (Pseudoceratinidae, Verongiida). *Marine Drugs*, 17, 92–109.
 595 <https://doi.org/10.3390/md17020092>

596 Shams, M. I., Ifuku, S., Nogi, M., Oku, T., & Yano, H. (2011). Fabrication of optically transparent chitin
 597 nanocomposites. *Appl Phys A*, 102, 325–331. <https://doi.org/10.1007/s00339-010-5969-5>

598 Singh, A., Dutta, P. K., Kumar, H., Kureel, A. K., & Rai, A. K. (2018). Synthesis of chitin-glucan-aldehyde-
 599 quercetin conjugate and evaluation of anticancer and antioxidant activities. *Carbohydrate Polymers*,
 600 193(February), 99–107. <https://doi.org/10.1016/j.carbpol.2018.03.092>

601 Tsai, C. C., Payne, G. F., & Shen, J. (2018). Exploring pH-Responsive, Switchable Crosslinking Mechanisms for
 602 Programming Reconfigurable Hydrogels Based on Aminopolysaccharides. *Chemistry of Materials*,
 603 30(23), 8597–8605. <https://doi.org/10.1021/acs.chemmater.8b03753>

604 Weaver, J. C., Milliron, G. W., Miserez, A., Evans-lutterodt, K., Herrera, S., Gallana, I., ... Kisailus, D. (2012).
 605 The Stomatopod Dactyl Club : A Formidable Damage-Tolerant Biological Hammer. *Science*, 336(June),
 606 1275–1280. <https://doi.org/10.1126/science.1218764>

607 Wysokowski, M., Petrenko, I., Stelling, A. L., Stawski, D., Jesionowski, T., & Ehrlich, H. (2015). Poriferan
 608 chitin as a versatile template for extreme biomimetics. *Polymers*, 7, 235–265.
 609 <https://doi.org/10.3390/polym7020235>

610 Xu, H., Nishida, J., Wu, H., Kobayashi, M., Otsuka, H., & Takahara, A. (2012). Competition between
 611 Oxidation and Coordination in Cross-Linking of Polystyrene Copolymer Containing Catechol Groups.
 612 *ACS Macro Lett.*, 1, 457–460. <https://doi.org/10.1021/mz200217d>

613 Xu, J., Strandman, S., Zhu, J. X. X., Barralet, J., & Cerruti, M. (2015). Genipin-crosslinked catechol-chitosan
 614 mucoadhesive hydrogels for buccal drug delivery. *Biomaterials*, 37, 395–404.
 615 <https://doi.org/10.1016/j.biomaterials.2014.10.024>

616 Xu, Z. (2013). Mechanics of metal-catecholate complexes: the roles of coordination state and metal types.
 617 *Scientific Reports*, 3, 2914. <https://doi.org/10.1038/srep02914>

618 Yang, S. S., Chen, Y. di, Zhang, Y., Zhou, H. M., Ji, X. Y., He, L., ... Wu, W. M. (2019). A novel clean production
 619 approach to utilize crop waste residues as co-diet for mealworm (*Tenebrio molitor*) biomass
 620 production with biochar as byproduct for heavy metal removal. *Environmental Pollution*, 252, 1142–

621 1153. <https://doi.org/10.1016/j.envpol.2019.06.028>

622 Zhu, K., Tu, H., Yang, P., Qiu, C., Zhang, D., Lu, A., ... Zhang, L. (2019). Mechanically Strong Chitin Fibers with
 623 Nanofibril Structure, Biocompatibility, and Biodegradability. *Chemistry of Materials*, 31(6), 2078–2087.
 624 <https://doi.org/10.1021/acs.chemmater.8b05183>

625 Zhu, K. Y., Merzendorfer, H., Zhang, W., Zhang, J., & Muthukrishnan, S. (2016). Biosynthesis, Turnover, and
 626 Functions of Chitin in Insects. *Annual Review of Entomology*, 61, 177–196.
 627 <https://doi.org/10.1146/annurev-ento-010715-023933>

628 Zvarec, O., Purushotham, S., Masic, A., Ramanujan, R. V, & Miserez, A. (2013). *Catechol-Functionalized*
 629 *Chitosan/Iron Oxide Nanoparticle Composite Inspired by Mussel Thread Coating and Squid Beak*
 630 *Interfacial Chemistry*.

631

632